Appl. Phys. A 84, 403–407 (2006)
DOI: 10.1007/s00339-006-3645-6

Applied Physics A
Materials Science & Processing

S. KARIM[1,✉]
M.E. TOIMIL-MOLARES[2]
F. MAURER[3]
G. MIEHE[3]
W. ENSINGER[3]
J. LIU[4]
T.W. CORNELIUS[2]
R. NEUMANN[2]

Synthesis of gold nanowires with controlled crystallographic characteristics

[1] Department of Chemistry, Philipps University, Marburg, Germany
[2] Gesellschaft für Schwerionenforschung (GSI), Darmstadt, Germany
[3] Institute of Materials Science, Darmstadt University of Technology, Darmstadt, Germany
[4] Institute of Modern Physics, Chinese Academy of Sciences (CAS), Lanzhou, P.R. China

Received: 13 February 2006/Accepted: 2 June 2006
Published online: 4 July 2006 •

ABSTRACT The controlled fabrication of poly- and single-crystalline Au nanowires is reported. In polycarbonate templates, prepared by heavy-ion irradiation and subsequent etching, Au nanowires with diameters down to 25 nm are electrochemically synthesized. Four-circle X-ray diffraction and transmission electron microscopy measurements demonstrate that wires deposited potentiostatically at a voltage of −1.2 V at 65 °C are single-crystalline and oriented along the [110] direction. By reverse-pulse electrodeposition, wires oriented along the [100] direction are grown. The wires are cylindrical over their whole length. The morphology of the caps growing on top of poly- and single-crystalline wires is a strong indication of the particular crystalline structure of the nanowires.

PACS 61.46.-w; 81.07.-b

1 Introduction

Gold nanowires have potential applications in fields such as optoelectronics and sensorics. On the one hand, for example, recent studies demonstrated the non-diffraction limited light transport by gold nanowires [1]. Several works have been devoted to the investigation of surface plasmon polariton (SPP) waves of gold nanowires on a substrate. The aim is to manipulate and transmit light on the nanoscale by exciting and guiding SPPs along metal/insulator interfaces, and finally transforming them back into free-propagating light [1–4]. A practical implementation of nanowire-based devices would allow a significant decrease in size of opto–electronic elements. On the other hand, the chemical stability of Au wires and the possibility of selectively attaching biomolecules to their walls, open up their potential use as biological sensors [5, 6].

There exist several techniques for the production of gold nanowires, e.g., chemical vapor deposition and photochemical, electroless, and electrochemical deposition [7–13]. Electrochemical deposition in combination with templates is both versatile and suitable for large-scale production of nanowires with well-defined shape and crystalline characteristics, highly needed for nanowire applications [14–16]. Different templates are available such as porous anodic alumina films, etched ion-track membranes (EITM), mesoporous silica, and porous glass. We selected EITM because they make it possible to independently vary length, size, and geometry of the wires. Another unique advantage is the possibility of choosing the density of pores from 10^{10} cm^{-2} down to a single pore per membrane, enabling thus the fabrication of large, dense nanowire arrays as well as single nanowires. Single nanowires can be reliably contacted by sputtering of a second electrode to investigate their electrical properties as a function of material, shape, and size [17, 18].

As demonstrated earlier, the structure of nanowires can be tuned from poly- to single-crystalline by carefully varying the electrodeposition parameters [7, 15, 19]. This article reports the synthesis of Au wires with controlled crystallographic characteristics. By varying the deposition conditions, we systematically fabricated both poly- and single-crystalline wires. In addition, the preferred crystallographic orientation of the wire arrays was adjusted by controlling the voltage signal.

2 Experimental

Polycarbonate foils with thickness 30 μm (Bayer AG, Leverkusen) were irradiated at the UNILAC linear accelerator of GSI with U ions of kinetic energy ~ 2 GeV, applying irradiation fluences around 10^8–10^9 ions/cm^2. Nanoporous track templates were then produced by chemically etching the ion tracks in a 6 M NaOH solution at 50 °C. Prior to etching, each foil was irradiated with UV light for 2 h to increase the track-etching sensitivity (track-to-bulk etching ratio), thus favoring the fabrication of pores with cylindrical geometry [20]. The diameter of the etched pores was controlled by the etching time. A conductive Cu layer was deposited on one membrane side and acted as cathode during electrodeposition, which was performed in an electrochemical two-compartment cell [17, 18]. During electrodeposition, the current was recorded as a function of time. The process was stopped when the wire length reached the desired value, as calculated from the deposited charge using Faraday's law. A commercial gold bath of potassium dicyanoaurate(I) Puramet 402 (Doduco company) containing 10 g/l of gold was employed as electrolyte, and a Au rod acted as anode.

✉ Fax: (49)6159-712179, E-mail: s.karim@gsi.de

If the deposition process was continued once the wires reached the membrane surface, caps grew on top. The morphology of wires and caps was investigated by scanning electron microscopy (SEM). We studied the crystalline orientation of the wires by X-ray diffraction (XRD) while keeping the wires embedded in the membrane. This investigation was performed at a STOE four-circle diffractometer using Co $K_{\alpha 1}$ radiation ($\lambda = 1.78897$ Å). In addition, after dissolution of the polymer matrix in dichloromethane, transmission electron microscopy (TEM) and selected-area electron diffraction (SAED) were employed to investigate the crystallographic structure of the nanowires.

3 Results and discussion

SEM and high-resolution (HR) SEM images in Fig. 1a and b display Au wires with diameters 160 nm and

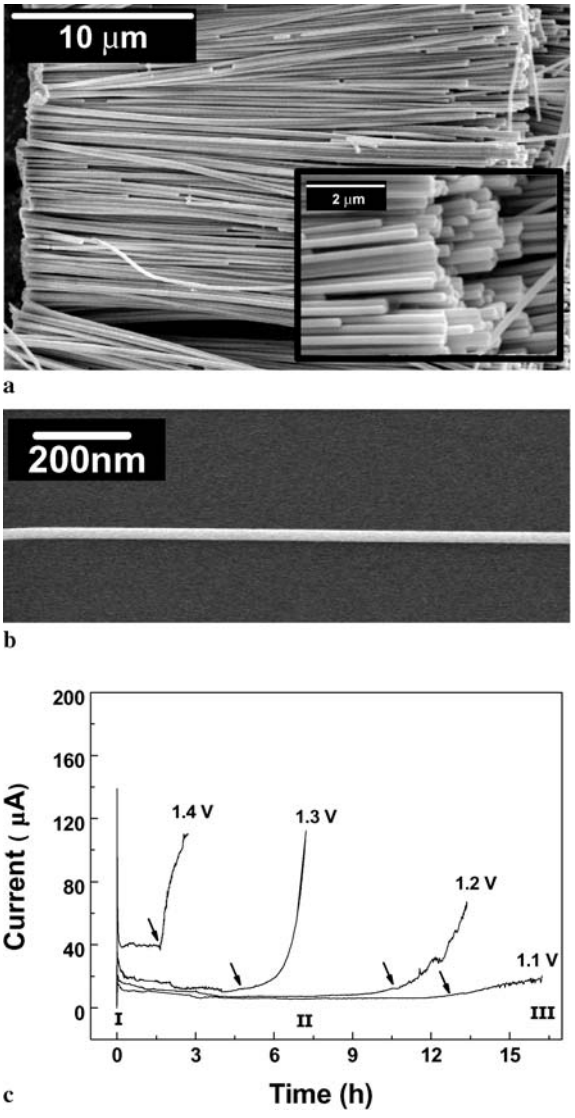

FIGURE 1 (**a**) SEM picture of 160 nm diameter gold wires. *Inset*: end sections of wires; (**b**) HRSEM micrograph of a 25 nm wire; (**c**) current–time curves for Au electrodeposition in membranes with 70 nm diameter pores for different potentiostatic voltages at 65 °C. *Arrows* indicate the end of zone II, i.e., the point at which the current starts to increase

U (V)	Q_{theo} (C)	Q_{exp} (C)	Q_{exp}/Q_{theo} (%)	j (mA/cm^2)
1.1	0.49	0.33	66.32	0.34
1.2	0.49	0.36	72.89	0.42
1.3	0.49	0.32	64.21	1.03
1.4	0.49	0.23	43.88	2.25

TABLE 1 Data extracted from Fig. 1c for electrodeposition of 70 nm Au wires. Q_{theo} is calculated using Faraday's law

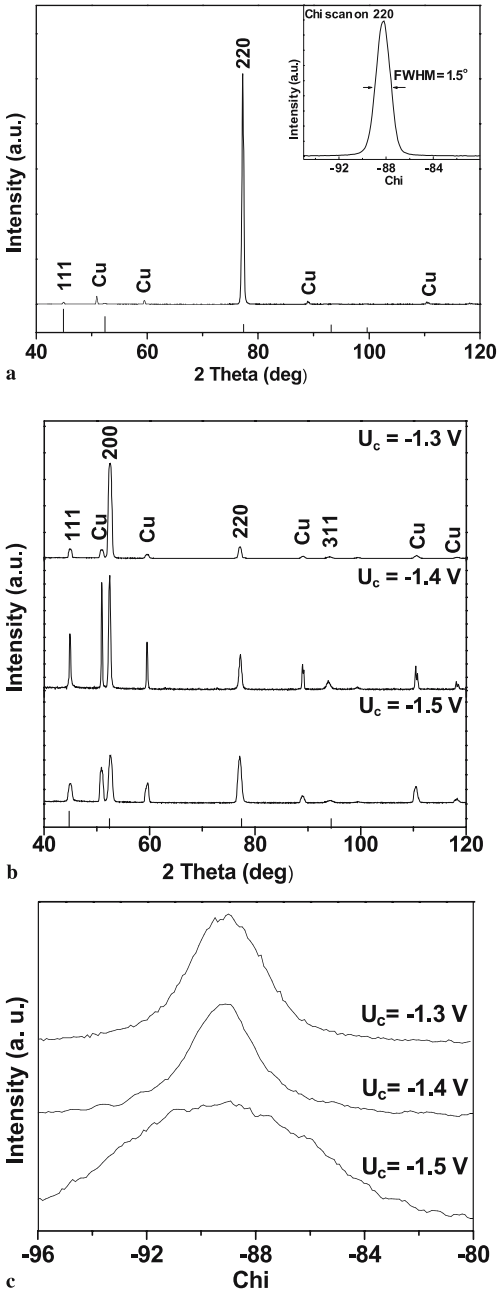

FIGURE 2 XRD patterns for 70 nm Au nanowires. *Vertical lines* drawn at the abscissa in Fig. 2a and b represent the reflections from a powdered Au sample. (**a**) Potentiostatical deposition at -1.2 V and 65 °C (*inset* shows the corresponding rocking curve on (110) reflection); (**b**) deposition under reverse pulse condition with different cathodic voltages at 65 °C. In all measurements, $U_a = -400$ mV, $t_a = 1$ s, $t_c = 6$ s; (**c**) rocking curves on (100) reflection for the conditions mentioned in (**b**)

25 nm, respectively, grown under potentiostatic conditions. Independent of diameter, the nanowires possess homogenous contours and are cylindrical in shape. The inset of Fig. 1a shows a magnified image of end sections of wires in Fig. 1a revealing that the wires are cylindrical with uniform cross-section over the whole length. Since the deposited material acquires exactly the same shape as the pore, the characteristics of membranes employed are extremely important for the fabrication of nanowires. The shape of the pores in commercially available membranes is, in general, not cylindrical with a constant cross-section but is rather toothpick- or cigar-like [21]. Resultantly, the wires prepared using the commercial membranes are reported to be up to a factor 2.5 wider in the middle than at the end [22]. Measurements by SEM and TEM of wires prepared in our experiments did not reveal any diameter variation beyond 10% along the whole length. The irradiation with UV light prior to etching proved crucial in obtaining cylindrical wires. Templates fabricated without UV sensitization were found to contain pores with rather large diameter variation. In addition, no surfactants were added to the etching solution, which are also known to considerably influence the pore shape [23].

Figure 1c displays the current-vs.-time curves recorded during electrodeposition of Au nanowires of 70 nm diameter at different voltages and 65 °C. The shape of the curves is in agreement with the behavior described previously for copper deposition in templates [15]. The higher the voltage, the larger is the current density and, as expected by Faraday's law, the shorter the time needed to completely fill the pores. In Table 1, Q_{theo} is the charge calculated by Faraday's law, Q_{exp} is the integral of the $I(t)$ curves from the beginning of the deposition ($t = 0$) to the end of zone II (see arrows in Fig. 1c), and j is the current density calculated by taking in all cases the current value approximately in the middle of zone II. The ratio $Q_{\text{exp}}/Q_{\text{theo}}$ amounts to 0.6–0.7 for voltages U between -1.1 and -1.3 V. Assuming 100% current efficiency, we find that $Q_{\text{exp}}/Q_{\text{theo}}$ indicates that the maximum percentage of pores filled under the conditions employed in this work ranges between 65 and 72%, which is a reasonably good value taking into account both the uncertainties included in Q_{theo} (namely wire length, wire diameter, and fluence) and the hydrophobicity of the polycarbonate. For $U = -1.4$ V, the ratio $Q_{\text{exp}}/Q_{\text{theo}}$ is lower. This is due to the very fast and inhomogeneous deposition taking place at higher voltages. In this case, the current increases very rapidly as soon as the first wire reaches the surface, while the other pores remain partially or completely empty.

Figure 2a displays the X-ray diffractogram of a gold nanowire array deposited under potentiostatic conditions, applying $U = -1.2$ V at $T = 65$ °C. The reflections were identified and compared with those of a polycrystalline Au sample, drawn as vertical lines at the abscissa of the Fig. 2a [24]. It is obvious from the diffractogram that the nanowires grown with cyanidic electrolyte under these conditions have a very high degree of crystalline orientation. To quantitatively determine the degree of orientation, we used the texture coefficient (TC):

$$\mathrm{TC}(hkl)_i = \frac{\dfrac{I(hkl)_i}{I_0(hkl)_i}}{\dfrac{1}{N}\sum_n \dfrac{I(hkl)_n}{I_0(hkl)_n}},$$

where $I(hkl)_i$ is the observed intensity of the $(hkl)_i$ plane and $I_0(hkl)_i$ is the intensity of the $(hkl)_i$ reflection of a polycrystalline Au sample. N is the total number of reflections taken into account. TC values larger than 1 would indicate a preferred orientation of the wires in the array. $\mathrm{TC} = N$ is the highest possible value and would indicate that all wires possess the same orientation.

For nanowires created under the above mentioned conditions, $\mathrm{TC}[110] = 4.8$ ($N = 5$), indicating a nearly perfect orientation of the nanowires along the [110] direction. The rocking curve measured on the (110) reflection (inset Fig. 2a) possesses a FWHM of only 1.5°, once again demonstrating the high degree of texture of the wires. Figure 2b shows the XRD patterns of the nanowires fabricated under reverse pulse conditions by applying cathodic voltages $U_c = -1.3$, -1.4, and -1.5 V. In all cases, the anodic voltage U_a was fixed at 0.4 V, while the cathodic t_c and anodic t_a cycles had a length of 6 and 1 s, respectively. In all cases, the Au nanowires possess a preferred orientation in the [100] direction, TC[100] amounting to 3.8, 2.7, and 1.6 for cathodic voltages -1.3, -1.4, and -1.5 V, respectively ($N = 5$). The FWHM of the rocking curve of [100] reflection correspond-

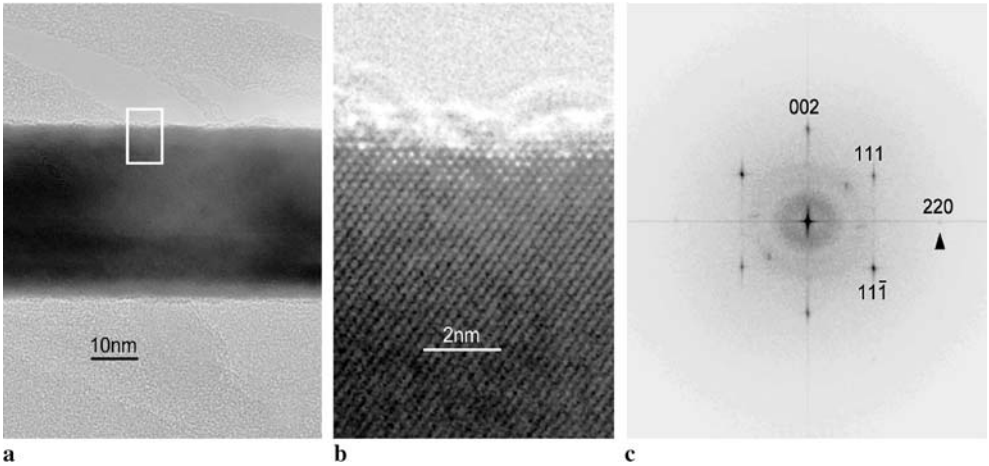

FIGURE 3 HRTEM image of a single-crystalline gold nanowire. (**a**) Low magnification; (**b**) enlargement of the *framed area* in (**a**), zone [−1 1 0]; (**c**) Fourier transform of (**b**)

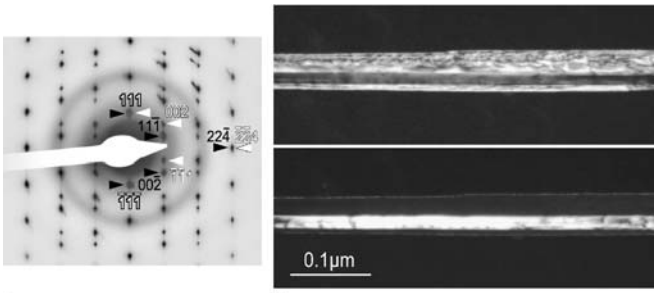

a b

FIGURE 4 (**a**) SAED pattern of a (111)-twin. *Black* and *white arrows* point to reflections of the respective orientations. The wire is tilted by ≈ 30° from the horizontal position. (**b**) Dark-field images with reflection 1 1 −1 (*top*) and −1 −1 1 (*bottom*)

ingly increases at higher voltages. It amounts to 3.2°, 2.8°, and 8.6° at $U_c = -1.3, -1.4$, and -1.5 V, respectively (Fig. 2c). On the other hand, while TC[100] decreases, TC[110] increases with higher cathodic voltages, being 0.7, 0.9, and 2.6 for voltages −1.3, −1.4, and −1.5 V. The reason for different preferred orientations for potentiostatic and reverse pulse deposition is not yet clear, but similar results have been reported recently for Bi nanowires [19]. As in the case of Bi nanowires, we expect that the orientation of wires grown with longer cathodic cycles and lower anodic potentials also approaches that of wires grown by potentiostatic deposition.

Figure 3 shows the HRTEM image of a single-crystalline wire grown at $U = -1.2$ V and $T = 65$ °C. Low-and high-magnification images, a and b, as well as the Fourier transform c of Fig. 3b evidence the (110) orientation. Generally, no grain boundaries were observed by TEM. Analysis with SAED confirmed the single-crystallinity and [110] growth direction as found by XRD. Growth of Au nanowires with [111] orientation during electrodeposition in track-etched polymeric templates has been reported [7]. The authors used a commercial orotemp electrolyte diluted in water with gelatin addition. The different commercial electrolyte and the presence of gelatin may influence the growth direction. Indeed, the authors reported that gelatin had a strong influence, no single-crystalline nanowires being obtained without the addition of gelatin. Within similar studies, Wang et al. reported that only wires oriented along the [111] and [11$\bar{2}$] directions contained twinned crystals, while no twins were found for wires growing along the [110] or [100] directions [25]. In our case, using the puramet cyanidic electrolyte, without gelatin addition, under potentiostatic conditions at 65 °C, (111)-twins oriented along the [110] direction were found. Figure 4 shows the diffraction pattern (a) and two oriented dark-field images (b) of a wire containing a lengthwise twin. The micrographs in b were acquired using reflections [11 − 1] (top) and [−1 − 11] (bottom). The extension of the wires in these images seems to be along (112), because the specimen had to be tilted by ≈ 30° to receive the zone [011]. The angle between [011] and [112] is 30°. Twins have been found also for copper nanowires with [110] orientation [26].

It was found that the cap growing on top, when a wire protrudes from the template, strongly evidences a particular crystallinity [27]. A great variety of faceted caps is formed during deposition. Figure 5a shows a cap grown on a single-crystalline wire deposited at −1.2 V, and 65 °C. The caps of

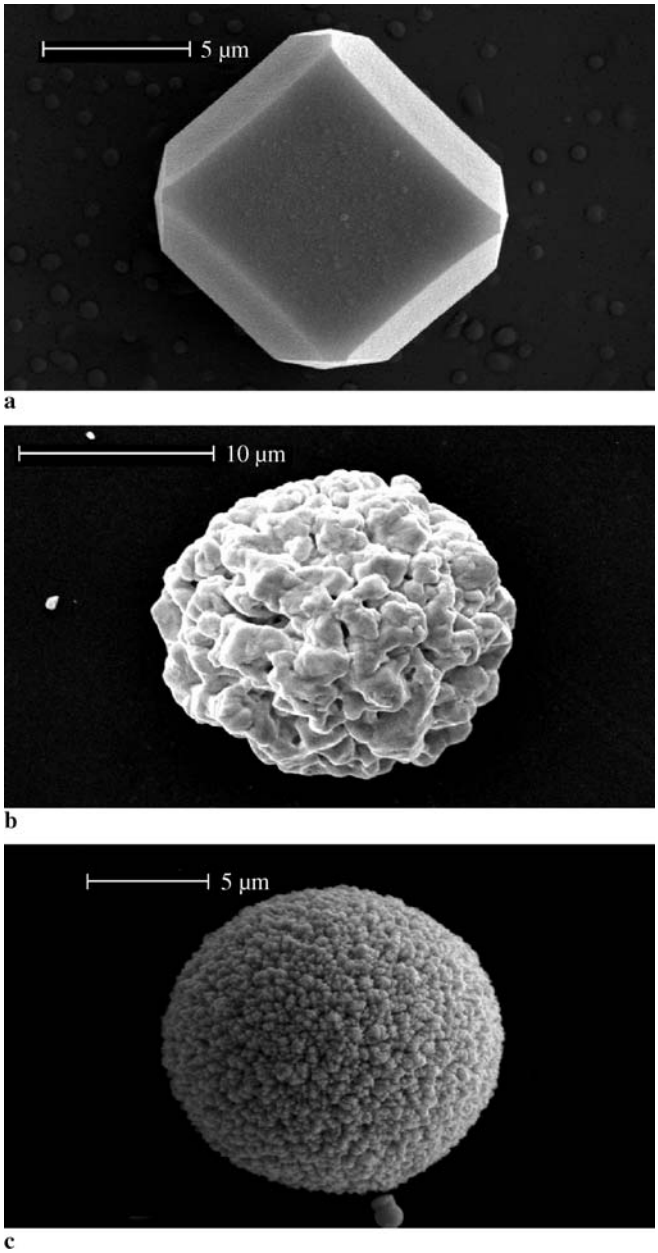

a b c

FIGURE 5 SEM images of caps grown on top of a Au nanowire. (**a**) Facetted single-crystalline cap formed during deposition of nanowires at −1.2 V and 65 °C; (**b**) hemispherical polycrystalline cap deposited with cyanide electrolyte at −1.5 V and 65 °C; (**c**) polycrystalline cap deposited with a commercial ammonium sulphite gold (I) electrolyte at −0.6 V and 50 °C

polycrystalline wires are hemispherical. A polycrystalline cap formed at −1.5 V and 65 °C is shown in Fig. 5b. The higher voltage favors the formation of new nuclei, thus promoting the growth of polycrystalline structures. The shape and morphology of both the wires and caps depend also strongly on the electrolyte. Potentiostatic deposition of gold nanowires with a commercial ammonium sulphite gold (I) electrolyte (Metakem) (gold content = 15 g/l), as shown in Fig. 5c, results in fine-grained caps, in contrast to coarse-grained caps formed with cyanidic electrolyte in Fig. 5b. Therefore, the structure of a cap provides indirect information about the wire crystallinity also in cases in which XRD and TEM analyses

are not possible, or where dissolution of the templates is not desired.

4 Conclusions

Both the potentiostatic and reversed pulse deposition of Au nanowires in polymeric templates together with different voltages and temperatures provide a suitable way to manipulate the crystallographic orientation of the nanowires. The wires can be varied in a well-controlled way from poly- to single-crystalline as well as generated with different crystallographic orientations. XRD and TEM analyses prove that the nanowires fabricated potentiostatically with potassium dicyanoaurate(I) electrolyte at 65 °C and -1.2 V are single-crystalline and oriented along the [110] direction. The nanowires deposited with reverse pulse have preferred orientation along the [100] direction, the texture coefficient being maximum at $U_c = -1.3$ V and decreasing with increasing U_c. All wires are cylindrical and no cigar- or tooth-pick-like geometry was found. The cap morphology strongly depends on the wire crystallinity and provides indirect information about the crystalline structure of nanowires.

ACKNOWLEDGEMENTS One of the authors (S.K.) expresses his gratitude to the Higher Education Commission, Pakistan, for providing a scholarship.

REFERENCES

1 J.R. Krenn, B. Lamprecht, H. Ditlbacher, G. Schider, M. Salerno, A. Leitner, F.R. Aussenegg, Europhys. Lett. **60**, 663 (2000)
2 J. Weeber, A. Dereux, C. Girarad, J.R. Krenn, J. Goudonnet, Phys. Rev. B **60**, 9061 (1999)
3 W.L. Barnes, A. Dereux, T.W. Ebbesed, Nature **424**, 824 (2003)
4 R.M. Dickson, L.A. Lyon, J. Phys. Chem. B **104**, 6095 (2000)
5 M. El-Kouedi, C.D. Keating, in *Nanobiotechnology, Concepts, Applications and Perspectives*, ed. by C.M. Niemeyer, C.A. Mirkin (Wiley-VCH, 2004), pp. 429–443
6 D.H. Reich, M. Tanase, A. Hultgren, L.A. Bauer, C.S. Chen, G.J. Meyer, J. Appl. Phys. **93**, 7275 (2003)
7 M. Tian, J. Wang, J. Kurtz, T.E. Mallouk, M.H.W. Chan, Nano Lett. **3**, 919 (2003)
8 M. Wirtz, C.R. Martin, Adv. Mater. **15**, 455 (2003)
9 X.Y. Zhang, L.D. Zhang, Y. Lei, L.X. Zhao, Y.Q. Mao, J. Mater. Chem. **11**, 1732 (2001)
10 W.B. Zhao, J.J. Zhu, H.Y. Chen, J. Cryst. Growth **258**, 176 (2003)
11 J. Gu, J. Shi, L. Xiong, H. Chen, L. Li, M. Ruan, Solid State Sci. **6**, 747 (2004)
12 P. Forrer, F. Schlottig, H. Siegenthaler, M. Textor, J. Appl. Electrochem. **30**, 533 (2000)
13 H. Araki, A. Fukuoka, Y. Sakamoto, S. Inagaki, N. Sugimoto, Y. Fukushima, M. Ichikawa, J. Mol. Catal. A Chem. **199**, 95 (2003)
14 C.R. Martin, Science **266**, 1961 (1993)
15 M.E. Toimil-Molares, V. Buschmann, D. Dobrev, R. Neumann, R. Scholz, I.U. Schuchert, J. Vetter, Adv. Mater. **13**, 62 (2001)
16 G. Yi, W. Scharzacher, Appl. Phys. Lett. **74**, 1746 (2000)
17 M.E. Toimil-Molares, N. Chtanko, T.W. Cornelius, D. Dobrev, I. Enculescu, R.H. Blick, R. Neumann, Nanotechnology **15**, S201 (2004)
18 N. Chtanko, M.E. Toimil-Molares, T.W. Cornelius, D. Dobrev, R. Neumann, J. Phys. Chem. B **108**, 9950 (2004)
19 T.W. Cornelius, J. Brötz, N. Chtanko, D. Dobrev, G. Miehe, R. Neumann, M.E. Toimil-Molares, Nanotechnology **16**, S246 (2005)
20 Z. Zhu, Y. Maekawa, H. Koshikawa, Y. Suzuki, N. Yonezawa, M. Yoshida, Nucl. Instrum. Methods Phys. Res. B**217**, 449 (2004)
21 E. Ferain, R. Legras, Nucl. Instrum. Methods Phys. Res. B **174**, 116 (2001)
22 C. Schönenberger, B.M.I. van der Zande, L.G.J. Fokkink, M. Henny, C. Schmid, M. Krueger, A. Bachtold, A. Huber, H. Birk, U. Staufer, J. Phys. Chem. B **101**, 5497 (1997)
23 P.Y. Apel, I.V. Blonskaya, O.L. Orelovich, S.N. Akimenko, B. Sartowska, S.N. Dmitriev, Colloid J. **66**, 725 (2004)
24 STOE Peak File C85-1330.pks
25 J. Wang, M. Tian, T.E. Mallouk, M.H.W. Chan, J. Phys. Chem. B **108**, 841 (2004)
26 M.E. Toilmil-Molares, private communication
27 M.E. Toimil-Molares, J. Brötz, V. Buschmann, D. Dobrev, R. Neumann, R. Scholz, I.U. Schuchert, C. Trautmann, J. Vetter, Nucl. Instrum. Methods Phys. Res. B **185**, 192 (2001)